


Generalized \mathcal{PT} Symmetry in Non-Hermitian Wireless Power Transfer Systems

Yuhao Wu^①, Lei Kang^{①,*} and Douglas H. Werner^{①,†}

Department of Electrical Engineering, The Pennsylvania State University, University Park, Pennsylvania 16802, USA

 (Received 19 May 2022; revised 18 September 2022; accepted 6 October 2022; published 8 November 2022)

We show that, by using a saturable gain g_{sat} , generalized \mathcal{PT} (GPT) symmetry can be achieved in the intrinsically unbalanced (non- \mathcal{PT} -symmetric) high-order wireless power transfer systems. A topology decomposition approach is implemented to analyze the parity of the high-order wireless power transfer systems. In the coupling parametric space, a global GPT -symmetric eigenstate is observed along with the spontaneous phase transition of the local GPT -symmetric eigenstates on the exceptional contour. GPT symmetry guarantees a highly efficient and stable power transfer across the distinct coupling regions, which introduces a new paradigm for a broad range of application scenarios involving asymmetric coupling.

DOI: 10.1103/PhysRevLett.129.200201

Existing wireless power transfer (WPT) systems can be categorized into two groups, i.e., radiative transfer [1] and nonradiative near-field transfer. The latter corresponds to typical non-Hermitian systems, including inductive [2–5] or resonance-based [6–9] WPT schemes, which constitute the majority of systems in practical use owing to their superior efficiency. However, for nonradiative WPT systems, a high efficiency is maintained only when the power transfer distance is comparable to the dimensions of the transmitting and the receiving components. The current nonradiative WPT schemes suggest a lack of robustness to variations in the application conditions. On the other hand, parity-time (\mathcal{PT}) symmetry [10–13] opens up a new perspective in the study of non-Hermitian systems in which gain and loss are the key to optimal resonance performance in different environmental conditions. \mathcal{PT} symmetry has been extensively explored in different fields [14–25] and recently has been exploited to enable robust WPT systems with high efficiency [1,26–30].

In the previous \mathcal{PT} WPT investigation, the \mathcal{PT} symmetry can only be realized either in a second order (two-body) system of balanced gain and loss rate ($\gamma = g$) [1,26,28,30], or in a third order (three-body) system of balanced coupling rates ($\kappa_{12} = \kappa_{23}$) [29]. Those systems suffer from two limitations. First, they rely on an inherently balanced coupling configuration. Second, due to the spontaneous symmetry breaking, high power efficiency can only be achieved locally in the strong coupling (SC) region at “ \mathcal{PT} -symmetric phase.” Therefore, the construction of a global \mathcal{PT} symmetry in WPT systems is not only important to achieve globally optimal power transfer efficiency, but also to understand the topological properties of intrinsically asymmetric non-Hermitian systems.

In this Letter, we theoretically demonstrate generalized parity-time (GPT) symmetry in high-order non-Hermitian asymmetric WPT systems. By applying a two-step parity

decomposition approach, the topology correlation between the three-body and two-body \mathcal{PT} -symmetric WPT systems is analyzed. The GPT -symmetric states are described as *on-band* steady states in a high dimensional parametric space ($\gamma, g, \kappa_{12}, \kappa_{23}$), with a saturation gain g_{sat} . Accordingly, a band theory interpretation is developed to analyze the *off-band* efficiency-compromised states with respect to the band surface, i.e., $g_{\text{sat}}(\gamma, \kappa_{12}, \kappa_{23})$ in the parametric space. Meanwhile, a maximized and stable power efficiency is guaranteed by a global GPT -symmetric state over both the weak coupling (WC) and SC regions.

Here, the third order WPT system [Fig. 1(d)] is represented as a mutual-coupled resonance system consisting of a transmitter (Tx, resonator 1), an intermedicator

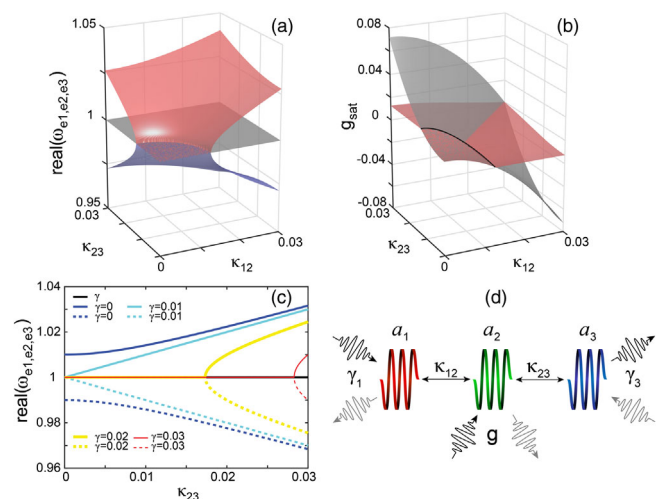


FIG. 1. GPT symmetric states in the parametric space. (a) Band surface of $\text{Re}(\omega_e)$ in $(\kappa_{12}, \kappa_{23})$ space. (b) g_{sat} of the eigenstates in $(\kappa_{12}, \kappa_{23})$ space. (c) Dynamics of exceptional point upon γ tuning. (d) Schematic of the high-order GPT symmetric wireless power transfer system.

(Ix, resonator 2), and a receiver (Rx, resonator 3). Each resonator is characterized by a resonance frequency (ω_1 , ω_2 , and ω_3) and a coupling rate (γ_1 , g , and γ_3). The coupling rate defined here is a theoretical aggregate of two components: (i) the interactional coupling rate representing the gain and loss from the coherent source and load outside the WPT system; and (ii) the intrinsic loss rate δ . The power interaction between the nearest resonators is described by the coupling rates κ_{12} and κ_{23} , which decrease exponentially with the increasing separation distance, d_{12} and d_{23} , between the resonators [28,29]. The dynamics of the system can be analyzed using temporal coupling mode theory [31], and may be further described by the following Hamiltonian [Eq. (1)], in which the eigenstates, $\mathbf{a} = (a_1, a_2, a_3)^T$, correspond to the complex amplitude of the energy stored in each resonator.

$$-i \frac{d}{dt} \mathbf{a} = \omega \mathbf{a} = H \mathbf{a},$$

$$H = \begin{pmatrix} \omega_1 - i\gamma_1 & \kappa_{12} & 0 \\ \kappa_{12} & \omega_2 - ig & \kappa_{23} \\ 0 & \kappa_{23} & \omega_3 + i\gamma_3 \end{pmatrix}. \quad (1)$$

$$\omega_{e1} = \omega_0, \quad \omega_{e2,3} = \omega_0 \pm \sqrt{\kappa_{23}^2 + \kappa_{12}^2 - \gamma^2}$$

$$g_{\text{sat}} = \gamma \frac{\kappa_{23}^2 - \kappa_{12}^2}{(\omega - \omega_0)^2 + \gamma^2}, \quad g_{\text{sat}1} = \frac{\kappa_{23}^2 - \kappa_{12}^2}{\gamma} \quad \text{or} \quad g_{\text{sat}2,3} = \gamma \frac{\kappa_{23}^2 - \kappa_{12}^2}{\kappa_{23}^2 + \kappa_{12}^2}. \quad (2)$$

Figure 1(a) illustrates the band surfaces of the three steady states, i.e., the eigenfrequency (real part, normalized to ω_0) in the parametric space of κ_{12} and κ_{23} , when $\gamma = 0.0125$. An exceptional contour is observed at $\kappa_{12}^2 + \kappa_{23}^2 - \gamma^2 = 0$, which divides the parametric space into the SC region ($\kappa_{12}^2 + \kappa_{23}^2 - \gamma^2 > 0$) and the WC region ($\kappa_{12}^2 + \kappa_{23}^2 - \gamma^2 < 0$). The second and third eigenfrequencies require $\kappa_{12}^2 + \kappa_{23}^2 - \gamma^2 \geq 0$, corresponding to the steady and \mathcal{PT} -symmetric states in the SC region. In other words, spontaneous symmetry breaking occurs as the second and third eigenstates enter the WC region. The first eigenstate sustains a global \mathcal{PT} symmetry in both regions. Therefore, in the SC region, a bifurcation phenomenon can be identified between three eigenstates, $(\omega_{e1}, g_{\text{sat}1})$, $(\omega_{e2}, g_{\text{sat}2})$, and $(\omega_{e3}, g_{\text{sat}3})$, while in the WC region, three eigenfrequencies coalesce into a unity value. Similar eigenstates coalescing inside the exceptional contour (the black curve at exceptional contour) can also be observed on the g_{sat} surface [Fig. 1(b)], where the red (gray) surface is the g_{sat} representative of the second and the third (first) eigenstates. Furthermore, the condition $g_{\text{sat}2,3} = g_{\text{sat}1} = 0$ along the diagonal direction in $(\kappa_{12}, \kappa_{23})$ space is attributed to the inherently symmetric condition, i.e., $\kappa_{12} = \kappa_{23}$ [29]. Namely, the \mathcal{PT} -symmetric condition is merely a special case in the $G\mathcal{PT}$ -symmetry system.

Considering the coherent coupling condition ($\omega_1 = \omega_2 = \omega_3 = \omega_0$) and a fixed and equal input and output rate at the source (γ_1) and the load (γ_3), i.e., $\gamma_1 = \gamma_3 = \gamma$, a characteristic equation can be obtained to determine the eigenstates of the WPT system, $|H - \omega| = (\omega_d - i\gamma) \times (\omega_d - ig)(\omega_d + i\gamma) - \kappa_{23}^2(\omega_d - i\gamma) - \kappa_{12}^2(\omega_d + i\gamma) = 0$. Here, $\omega_d = \omega_0 - \omega$. In contrast to the systems in previously reported studies [29], the WPT systems considered in this Letter are inherently asymmetric and can be defined by the asymmetric coupling rates, i.e., $\kappa_{12} \neq \kappa_{23}$. Importantly, a $G\mathcal{PT}$ symmetry can be reestablished by introducing a nonzero saturable gain g_{sat} into the intermediary. Based on the real frequency assumption, we observe that (i) the real part of the characteristic function can be separated to obtain three eigenfrequencies of the steady states [Eq. (2)]; and (ii) g_{sat} required can be derived from the imaginary part. Obviously, the formulation of g_{sat} is associated with the eigenfrequency. According to Eq. (2), when $\kappa_{12} < \kappa_{23}$, $g_{\text{sat}} > 0$, while, when $\kappa_{12} > \kappa_{23}$, $g_{\text{sat}} < 0$. g_{sat} serves as a measure of the asymmetric orientation of the system, indicating the functionality of g_{sat} in adjusting the symmetry property of the system.

This inclusion relation illustrates the generality of the $G\mathcal{PT}$ symmetry. Figure 1(c) illustrates the dynamics of the exceptional contour when $\kappa_{12} = 0.01$. Clearly, the exceptional point moves toward the zero as the input and output rate γ decreases. Moreover, if $\gamma < \kappa_{12}$, the spontaneous symmetry breaking (exceptional point) disappears due to a permanent SC condition ($\kappa_{12}^2 - \gamma^2 > 0$). Thus, the second and the third eigenstates can only be globally \mathcal{PT} symmetric at a limited input and output rate γ .

Here, the equivalence between the steady states and the $G\mathcal{PT}$ symmetry is rigorously illustrated. The time reversal operator is applied, i.e., $\hat{T}^\dagger t \hat{T} = -t$, to any time dependent physical quantities. The parity operator gives $\hat{P}^\dagger \hat{r} \hat{P} = -\hat{r}$, and can be applied to any coordinate related polar vectors. In principle, the \mathcal{PT} -symmetric Hamiltonian commutes with the combinative operation of $\hat{P} \hat{T}$. In the proposed three-body WPT system, the coordinate transformation ($\hat{r} \rightarrow -\hat{r}$) can be explicitly expressed as an index reversal from

$$(1, 2, 3) \rightarrow (3, 2, 1). \quad \text{The parity operator } \hat{P} = \begin{pmatrix} 0 & 0 & 1 \\ 0 & 1 & 0 \\ 1 & 0 & 0 \end{pmatrix}.$$

At the steady states, the transformation of the Hamiltonian under the simultaneous action of \hat{P} and \hat{T} can be derived as

$$\begin{aligned} \hat{\mathcal{P}} \hat{\mathcal{T}} H(\hat{r}, t) \hat{\mathcal{T}}^{-1} \hat{\mathcal{P}}^{-1} &= \hat{\mathcal{P}} H^*(\hat{r}, -t) \hat{\mathcal{P}}^{-1} = \hat{\mathcal{P}} \begin{pmatrix} \omega_0 + i\gamma & \kappa_{12} & 0 \\ \kappa_{12} & \omega_0 + ig_{\text{sat}}(\hat{r}) & \kappa_{23} \\ 0 & \kappa_{23} & \omega_0 - i\gamma \end{pmatrix} \hat{\mathcal{P}}^{-1} = H^*(-\hat{r}, -t) \\ &= \begin{pmatrix} \omega_0 - i\gamma & \kappa_{21} & 0 \\ \kappa_{21} & \omega_0 + ig_{\text{sat}}(-\hat{r}) & \kappa_{32} \\ 0 & \kappa_{32} & \omega_0 + i\gamma \end{pmatrix}. \end{aligned} \quad (3)$$

g_{sat} is odd symmetric, i.e., $-g_{\text{sat}}(\hat{r}) = g_{\text{sat}}(-\hat{r})$, which corresponds to a transformation from an input (gain) to an output (loss) interaction at the intermediary. Thus, $\hat{\mathcal{P}} \hat{\mathcal{T}} H(\hat{r}, t) \hat{\mathcal{T}}^{-1} \hat{\mathcal{P}}^{-1} = H(\hat{r}, t)$ is demonstrated, i.e., $[\hat{\mathcal{P}} \hat{\mathcal{T}}, H(\hat{r}, t)] = 0$. Physically speaking, the non-Hermitian Hamiltonian of the three-body WPT system is $\hat{\mathcal{P}} \hat{\mathcal{T}}$ invariant at its steady states.

From an evolutionary perspective, three-body WPT systems can be viewed as generalized two-body WPT systems, especially when $\kappa_{12} \neq \kappa_{23}$. Accordingly, the generalized parity reversal operation of the three-body system can be sequentially decomposed into one local and one global second order parity operation. One example ($\kappa_{12} < \kappa_{23}$) is presented in Fig. 2. Reasonably, the Tx is analogized as a ‘‘monopole’’ (red sphere) of positive input rate (gain), while the Ix and the Rx are collectively interpreted as a ‘‘dipole’’ with the polarity defined by the unbalanced input and output (in general, $g \neq \gamma$) at the two poles. Consequently, the generalized parity reversal operation $\hat{\mathcal{P}}$ can be intuitively decomposed into a global parity inversion ($\hat{\mathcal{P}}_G$) and a local parity inversion ($\hat{\mathcal{P}}_L$). $\hat{\mathcal{P}}_G = \sigma_x$ is based on the position inversion between the monopole and the dipole ($\hat{\mathcal{P}}_G^\dagger \hat{r}_G \hat{\mathcal{P}}_G = -\hat{r}_G$, corresponds to $[1, (2, 3)] \rightarrow [3, (1, 2)]$). $\hat{\mathcal{P}}_L = \sigma_x$ reverses the two polar ends of the dipole [$\hat{\mathcal{P}}_L^\dagger \hat{r}_L \hat{\mathcal{P}}_L = -\hat{r}_L$, corresponding to $(2, 3) \rightarrow (3, 2)$]. Meanwhile, $\hat{\mathcal{T}}^\dagger t \hat{\mathcal{T}} = -t$, is universal. Accordingly, the Hamiltonian of the three-body system is reformulated according to Eq. (4):

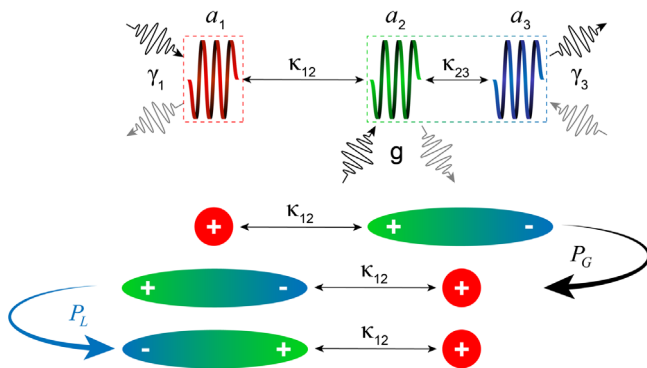


FIG. 2. Local and global parity decomposition of the general- ized parity based on a dipole-monopole analog.

$$H(\hat{r}_G, H_L, t) = \begin{pmatrix} \omega_0 - i\gamma & \kappa_{12} \\ \kappa_{12} & H_L(\hat{r}_L, t) \end{pmatrix}, \quad (4)$$

$$H_L(\hat{r}_L, t) = \begin{pmatrix} \omega_0 - ig & \kappa_{23} \\ \kappa_{23} & \omega_0 + i\gamma \end{pmatrix}, \quad (5)$$

where the local Hamiltonian H_L describes the dipole internal interaction under a local coordinate definition. Compared with the two-body WPT system [28], the three-body topology is equivalent to that of a global two-body topology embedded with a local two-body system at one pole, which suggests that a GPT -symmetric three-body topology and a PT -symmetric two-body topology are globally equivalent. Therefore, $\hat{\mathcal{P}}_G = \hat{\mathcal{P}}_L = \sigma_x$, which describes the coordinate inversion on different hierarchies of the system, aggregately controls the generalized parity of the third order system. Accordingly, the generalized PT symmetry of the three-body system can be demonstrated by a two-step parity operation and a universal time reversal operation (details are provided in Ref. [32]). Furthermore, this parity decomposition method can also be applied to high-order WPT systems (see detailed discussion in Ref. [32]).

In contrast to the coupling limitations observed in linear two-body systems [28], the GPT -symmetric states of the three-body configuration, $(\omega_{e1}, g_{\text{sat}1})$, $(\omega_{e2}, g_{\text{sat}2})$, and $(\omega_{e3}, g_{\text{sat}3})$, can achieve the maximum power transfer efficiency in both the WC and SC regions. In particular, the first steady state, $(\omega_{e1}, g_{\text{sat}1})$, is not only globally GPT symmetric, but also does not require an adaptive operating frequency across the distinct coupling regions. According to Eq. (6), each steady eigenstate, $\mathbf{a} = (a_1, a_2, a_3)^T$, with the corresponding saturable gain g_{sat} defines the theoretical limit of the power transfer efficiency of three-body WPT systems. Therefore, a band theory interpretation can be established in analogy to laser theory [28]. The imperfection of any efficiency-compromised states can be analyzed with respect to these ‘‘on-band’’ steady states.

$$\eta = \frac{\gamma_3 |a_3|^2}{\gamma_1 |a_1|^2 + g |a_2|^2}. \quad (6)$$

In 4D parametric space, the band surfaces of the steady states can be represented by $g_{\text{sat}}(\gamma, \kappa_{12}, \kappa_{23})$, while any imperfect state of a random coupling rate definition

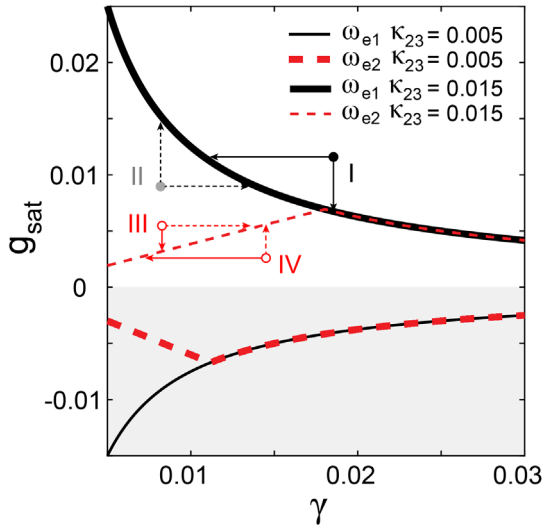


FIG. 3. Band theory interpretation of the WPT system in a high-dimensional parametric space $(g, \gamma, \kappa_{12}, \kappa_{23})$.

$(\gamma, g, \kappa_{12}, \kappa_{23})$ can be virtually denoted as a point in the space. For simplicity, we set $\kappa_{12} = 0.01$, $\kappa_{23} = 0.005$, and 0.015 . Thus, the band surface degenerates into a 2D curve, $g_{\text{sat}}(\gamma)$ [Fig. 3(b)]. The plot contains two coupling regions, the upper [lower (gray)] half under Rx-dominated (Tx-dominated) coupling, $\kappa_{12} < \kappa_{23}$ ($\kappa_{12} > \kappa_{23}$). In each half, the black (red dashed) curve denotes $g_{\text{sat}1}(\gamma)$ of the first steady state [$g_{\text{sat}2,3}(\gamma)$ of the second and the third steady states]. Importantly, a similar degeneracy between eigenstates can still be observed at the exceptional point.

When $\kappa_{12} > \kappa_{23}$, for a system of any fixed rate (γ, g) , there will be four states. If $g(\gamma) = g_{\text{sat}}(\gamma)$, the system operates *on band* with the maximum power transfer efficiency. Otherwise, state (γ, g) is an off-band state with a compromised efficiency. The first off-band state denoted by the black dot (I) corresponds to the oversaturated parameters of both γ and g , and is defined as the *oversaturated state*, which can be considered as an “excited state” induced by an external stimulation of rate g . This state can transit to an on-band “ground state” via either a “stimulated emission” (reduction in g indicated by the downward solid arrow) or a “momentum matching” (reduction in γ indicted by the leftward solid arrow). On the contrary, the state, represented by the gray dot (II), is categorized as the *unsaturated state*, which cannot directly transit to an on-band state without an extra “feed.” In addition, when the system satisfies either $g(\gamma) > g_{\text{sat}}(\gamma)$, $\gamma(g) < \gamma_{\text{sat}}(g)$ or $\gamma(g) > \gamma_{\text{sat}}(g)$, $g(\gamma) < g_{\text{sat}}(\gamma)$ [red circles (III) and (IV), respectively, in Fig. 3], it is at a hybrid state or a *semisaturated state*. A similar analysis can be implemented when $\kappa_{12} < \kappa_{23}$. Instructively, the power transfer efficiency across the parametric space can be derived by following this methodology.

With the loose coupling constraints, the *GPT* symmetry has immense potential for high-order WPT systems with

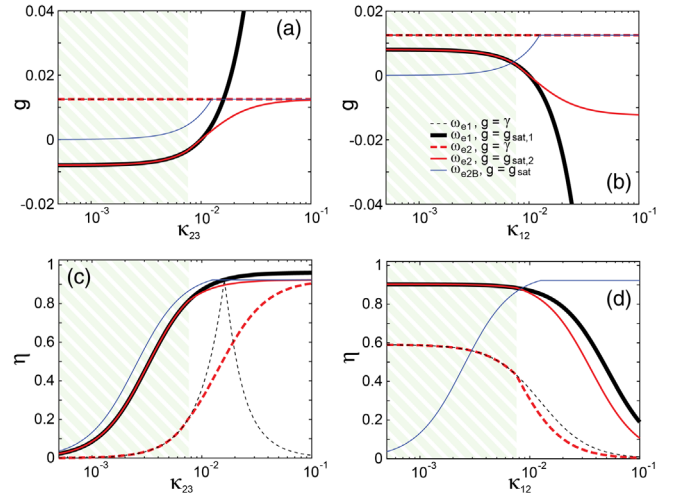


FIG. 4. WPT efficiency with different gain configurations g in a κ_{23} -dependent and κ_{12} -dependent system. (a) Static gain rate $g = \gamma = 0.0125$ and adaptive gain rate $g = g_{\text{sat}}$ for both κ_{23} -dependent systems operating at ω_{e1} and ω_{e2} . The WC range ($\kappa_{12}^2 + \kappa_{23}^2 - \gamma^2 < 0$) is highlighted by the shadowed area. (b) Same definition as (a) in a κ_{12} -dependent system. (c) WPT efficiency of the κ_{23} -dependent system under the corresponding gain rate in (a). (d) Same definition as (c) in a κ_{12} -dependent system.

greatly improved efficiency and practical feasibility. To further illustrate this, as shown in Fig. 4, we calculated the power efficiency η under different gain and loss rate schemes (g) with adaptive frequencies (i.e., eigenfrequencies). In this calculation, the distance between the Ix and the Tx (or Rx) was fixed, i.e., κ_{12} (or κ_{23}) = 0.01, while κ_{23} (or κ_{12}) is the only variable of the system. Operating at the first eigenfrequency $\omega = \omega_{e1}$, two gain scenarios, i.e., the static gain $g = \gamma = 0.0125$ and the adaptive gain $g = g_{\text{sat},1}$, are presented as the dashed and solid black curves, respectively, in both Figs. 4(a) and 4(b). Similarly, for $\omega = \omega_{e2}$, these two gain schemes are plotted as the dashed and solid red curves, respectively. In the same manner, the power transfer efficiencies under the corresponding gain schemes are presented in both Figs. 4(c) and 4(d). For comparison purposes, the highest efficiency of the two-body WPT system [blue curve in Figs. 4(c) and 4(d)] and the corresponding gain rate [blue curve in Figs. 4(a) and 4(b)] are also presented. An equal dissipation rate $\delta = 0.0005$ is applied to all terminals in the system: a loss model $(\delta_1, \delta_2, \delta_3) = (5, 5, 5) \times 10^{-4}$ is assigned for the three-body system and $(\delta_1, \delta_2) = (5, 5) \times 10^{-4}$ for the two-body system.

For a κ_{23} -dependent system, with an adaptive gain, $g = g_{\text{sat},1}$ or $g = g_{\text{sat},2}$, the system can operate on band at a *GPT*-symmetric state. In the WC region, the efficiencies of the first and second *GPT*-symmetric state (black and red solid curves) are identical due to the mode degeneracy [Fig. 4(c)]. Compared with the two-body system (blue curve), the three-body system shows lower WPT efficiency

in this region due to the lossy intermediary. As κ_{23} increases to the SC region, the first GPT -symmetric state exhibits optimal efficiency, while the efficiency of the second GPT -symmetric state achieves saturation at the highest value of the two-body system (blue curve). Otherwise, based on a static gain scenario ($g = \gamma$), the three-body WPT system functions at off band states with no GPT symmetry. Under this circumstance, a dramatic efficiency drop can be observed for both the states of ω_{e1} [black dashed curve in Fig. 4(c)] and ω_{e2} (red dashed curve) across the entire coupling range. As predicted by the band theory interpretation, the GPT -symmetric states (adaptive gain schemes) are superior to the non- \mathcal{PT} -symmetric states (static gain schemes) in terms of the global efficiency. Therefore, the intersection points of the black solid and dashed curves, at $g = g_{\text{sat},1} = \gamma$, indicate the maximum efficiency that can be attained under the static gain scheme. Furthermore, given the fact that $g = \gamma$ is an asymptote of $g_{\text{sat},2}$, the red dashed curve can only move close to the red solid efficiency curve.

On the other hand, for a κ_{12} -dependent system [Fig. 4(b)], the adaptive gain curves exhibit symmetric behavior (with respect to $g = 0$) compared with those of the κ_{23} -dependent system due to orientation reversal of the asymmetric configuration. The efficiency of the first and second GPT -symmetric states [red and black solid curve in Fig. 4(d)] dominate by 90% in the WC region. The observed efficiency distribution across the coupling range is complementary relative to that of the two-body system, which significantly enhances the power efficiency in the WC region. In particular, an up-to-90% power efficiency can now be achieved globally with the generalized \mathcal{PT} symmetry. Even the off-band state with a static gain rate [red and black dashed curve in Fig. 4(d)] can achieve a close-to-60% efficiency in the WC region. Furthermore, the GPT symmetry provides not only globally higher efficiency, but also an additional degree of freedom to tailor the corresponding loss profile based on the orientation of the system asymmetry (see detailed analysis in Sec. 4 in Ref. [32]). We note that, compared with the previously reported \mathcal{PT} -symmetric two-body and three-body systems, the proposed WPT system is primarily superior in two important aspects: (1) It requires no structural symmetry to realize an optimal WPT efficiency, and (2) it exhibits a globally GPT -symmetric state which is capable of sustaining high WPT efficiency without a frequency detuning (see Sec. 5 in Ref. [32]).

In conclusion, the generalized \mathcal{PT} symmetry of a third order WPT system has been proposed and demonstrated in non- \mathcal{PT} -symmetric WPT systems with a dynamic saturation gain. In principle, the similarity and difference between the topology of a three-body WPT system and its two-body counterparts are revealed via a parity operation decomposition. A transition between the \mathcal{PT} -symmetric phase and the broken phase was observed at the exceptional contour in the parametric space, with a concomitant mode degeneracy.

Importantly, a globally \mathcal{PT} -symmetric state, which possesses an optimal efficiency across the strong and weak coupling regions, was identified. Moreover, relative to the *on-band* GPT -symmetric states, a band theory interpretation was utilized to fully characterize the imperfect states in the parametric space. Our results show that GPT symmetry can significantly improve the robustness and efficiency of wireless power transfer systems under unbalanced coupling conditions. Furthermore, the intrinsic asymmetry configuration offers an additional degree of freedom for loss profile management.

The authors gratefully acknowledge support of this work by the John L. and Genevieve H. McCain endowed chair professorship at the Pennsylvania State University.

*To whom all correspondence should be addressed. lzk12@psu.edu

†To whom all correspondence should be addressed. dhw@psu.edu

- [1] A. Krasnok, D. G. Baranov, A. Generalov, S. Li, and A. Alù, Coherently Enhanced Wireless Power Transfer, *Phys. Rev. Lett.* **120**, 143901 (2018).
- [2] T.-H. Kim, G.-H. Yun, W. Lee, and J.-G. Yook, Highly efficient WPT system with negative impedance converter for Q -factor improvement, *IEEE Access* **7**, 108750 (2019).
- [3] Y. Cho, S. Lee, D.-H. Kim, H. Kim, C. Song, S. Kong, J. Park, C. Seo, and J. Kim, Thin hybrid metamaterial slab with negative and zero permeability for high efficiency and low electromagnetic field in wireless power transfer systems, *IEEE Transactions on Electromagnetic Compatibility* **60**, 1001 (2018).
- [4] B. Wang, K. H. Teo, T. Nishino, W. Yezunis, J. Barnwell, and J. Zhang, Experiments on wireless power transfer with metamaterials, *Appl. Phys. Lett.* **98**, 254101 (2011).
- [5] D. Huang, Y. Urzhumov, D. R. Smith, K. Hoo Teo, and J. Zhang, Magnetic superlens-enhanced inductive coupling for wireless power transfer, *J. Appl. Phys.* **111**, 064902 (2012).
- [6] A. Kurs, A. Karalis, R. Moffatt, J. D. Joannopoulos, P. Fisher, and M. Soljačić, Wireless power transfer via strongly coupled magnetic resonances, *Science* **317**, 83 (2007).
- [7] L. Li, X. Zhang, C. Song, and Y. Huang, Progress, challenges, and perspective on metasurfaces for ambient radio frequency energy harvesting, *Appl. Phys. Lett.* **116**, 060501 (2020).
- [8] S. Cheon, Y.-H. Kim, S.-Y. Kang, M. L. Lee, J.-M. Lee, and T. Zyung, Circuit-model-based analysis of a wireless energy-transfer system via coupled magnetic resonances, *IEEE Transactions on Industrial Electronics* **58**, 2906 (2011).
- [9] Y. Xie, Z. Zhang, Y. Lin, T. Feng, and Y. Xu, Magnetic quasi-bound state in the continuum for wireless power transfer, *Phys. Rev. Appl.* **15**, 044024 (2021).
- [10] L. Ge and A. D. Stone, Parity-Time Symmetry Breaking beyond One Dimension: The Role of Degeneracy, *Phys. Rev. X* **4**, 031011 (2014).

- [11] C. M. Bender and S. Boettcher, Real Spectra in Non-Hermitian Hamiltonians Having PT Symmetry, *Phys. Rev. Lett.* **80**, 5243 (1998).
- [12] C. M. Bender, D. C. Brody, and H. F. Jones, Complex Extension of Quantum Mechanics, *Phys. Rev. Lett.* **89**, 270401 (2002).
- [13] A. Mostafazadeh, Pseudo-Hermiticity and generalized PT- and CPT-symmetries, *J. Math. Phys. (N.Y.)* **44**, 974 (2003).
- [14] C. M. Bender, B. K. Berntson, D. Parker, and E. Samuel, Observation of PT phase transition in a simple mechanical system, *Am. J. Phys.* **81**, 173 (2013).
- [15] R. Fleury, D. Sounas, and A. Alù, An invisible acoustic sensor based on parity-time symmetry, *Nat. Commun.* **6**, 5905 (2015).
- [16] J. Schindler, A. Li, M. C. Zheng, F. M. Ellis, and T. Kottos, Experimental study of active LRC circuits with PT symmetries, *Phys. Rev. A* **84**, 040101(R) (2011).
- [17] S. Bittner, B. Dietz, U. Günther, H. L. Harney, M. Miski-Oglu, A. Richter, and F. Schäfer, PT Symmetry and Spontaneous Symmetry Breaking in a Microwave Billiard, *Phys. Rev. Lett.* **108**, 024101 (2012).
- [18] C. E. Rüter, K. G. Makris, R. El-Ganainy, D. N. Christodoulides, M. Segev, and D. Kip, Observation of parity-time symmetry in optics, *Nat. Phys.* **6**, 192 (2010).
- [19] K. G. Makris, R. El-Ganainy, D. N. Christodoulides, and Z. H. Musslimani, Beam Dynamics in PT Symmetric Optical Lattices, *Phys. Rev. Lett.* **100**, 103904 (2008).
- [20] X. Zhu, L. Feng, P. Zhang, X. Yin, and X. Zhang, One-way invisible cloak using parity-time symmetric transformation optics, *Opt. Lett.* **38**, 2821 (2013).
- [21] D. L. Sounas, R. Fleury, and A. Alù, Unidirectional cloaking based on metasurfaces with balanced loss and gain, *Phys. Rev. Appl.* **4**, 014005 (2015).
- [22] Y. Sun, W. Tan, H. Q. Li, J. Li, and H. Chen, Experimental Demonstration of a Coherent Perfect Absorber with PT Phase Transition, *Phys. Rev. Lett.* **112**, 143903 (2014).
- [23] M. Liertzer, L. Ge, A. Cerjan, A. D. Stone, H. E. Türeci, and S. Rotter, Pump-Induced Exceptional Points in Lasers, *Phys. Rev. Lett.* **108**, 173901 (2012).
- [24] M. Brandstetter, M. Liertzer, C. Deutsch, P. Klang, J. Schöberl, H. E. Türeci, G. Strasser, K. Unterrainer, and S. Rotter, Reversing the pump dependence of a laser at an exceptional point, *Nat. Commun.* **5**, 4034 (2014).
- [25] H. Hodaei, M.-A. Miri, M. Heinrich, D. N. Christodoulides, and M. Khajavikhan, Parity-time-symmetric microring lasers, *Science* **346**, 975 (2014).
- [26] Z. Zhu, H. Yuan, R. Zhang, A. Yang, X. Wang, and M. Rong, Parity-time symmetric model and analysis for stable multi-load wireless power transfer, *World Electr. Veh. J.* **12**, 226 (2021).
- [27] Z. Dong, Z. Li, F. Yang, C.-W. Qiu, and J. S. Ho, Sensitive readout of implantable microsensors using a wireless system locked to an exceptional point, *Nat. Electron.* **2**, 335 (2019).
- [28] S. Assaworarith, X. Yu, and S. Fan, Robust wireless power transfer using a nonlinear parity-time-symmetric circuit, *Nature (London)* **546**, 387 (2017).
- [29] C. Zeng, Y. Sun, G. Li, Y. Li, H. Jiang, Y. Yang, and H. Chen, High-order parity-time symmetric model for stable three-coil wireless power transfer, *Phys. Rev. Appl.* **13**, 034054 (2020).
- [30] C. Luo, D. Qiu, W. Gu, B. Zhang, Y. Chen, and W. Xiao, Multiload wireless power transfer system with constant output power and efficiency, *IEEE Trans. Ind. Appl.* **58**, 1101 (2022).
- [31] S. Fan, W. Suh, and J. D. Joannopoulos, Temporal coupled-mode theory for the Fano resonance in optical resonators, *J. Opt. Soc. Am. A* **20**, 569 (2003).
- [32] See Supplemental Material at <http://link.aps.org/supplemental/10.1103/PhysRevLett.129.200201> for details, which includes Refs. [33,34].
- [33] S. Assaworarith and S. Fan, Robust and efficient wireless power transfer using a switch-mode implementation of a nonlinear parity-time symmetric circuit, *Nat. Electron.* **3**, 273 (2020).
- [34] J. Zhou, B. Zhang, W. Xiao, D. Qiu, and Y. Chen, Nonlinear parity-time-symmetric model for constant efficiency wireless power transfer: Application to a drone-in-flight wireless charging platform, *IEEE Transactions on Industrial Electronics* **66**, 4097 (2019).